Results in Physics 6 (2016) 737–745

Contents lists available at ScienceDirect

Results in Physics

journal homepage: www.journals.elsevier.com/results-in-physics

Evolution of a novel Si-18Mn-16Ti-11P alloy in Al-Si melt and its influence on microstructure and properties of high-Si Al-Si alloy

Xiao-Lu Zhou, Xiang-Zhen Zhu, Tong Gao, Yu-Ying Wu *, Xiang-Fa Liu *

Key Laboratory for Liquid-Solid Structural Evolution and Processing of Materials, Ministry of Education, Shandong University, 17923 Jingshi Road, Jinan 250061, PR China

ARTICLE INFO

Article history:
Received 11 September 2016
Accepted 6 October 2016
Available online 14 October 2016

Keywords:
Hypereutectic Al-Si alloy
Primary Si
Refinement
AlP
Thermal expansion behavior
Si-18Mn-16Ti-11P master alloy

ABSTRACT

A novel Si-18Mn-16Ti-11P master alloy has been developed to refine primary Si to 14.7 ± 1.3 μm, distributed uniformly in Al-27Si alloy. Comparing with traditional Cu-14P and Al-3P, Si-18Mn-16Ti-11P provided a much better refining effect, with in-situ highly active AlP. The refined Al-27Si alloy exhibited a CTE of 16.25×10^{-6}/K which is slightly higher than that of Si_p/Al composites fabricated by spray deposition. The UTS and elongation of refined Al-27Si alloy were increased by 106% and 235% comparing with those of unrefined alloy. It indicates that the novel Si-18Mn-16Ti-11P alloy is more suitable for high-Si Al-Si alloys and may be a candidate for refining hypereutectic Al-Si alloy for electronic packaging applications. Moreover, studies showed that TiP is the only P-containing phase in Si-18Mn-16Ti-11P master alloy. A core-shell reaction model was established to reveal mechanism of the transformation of TiP to AlP in Al-Si melts. The transformation is a liquid-solid diffusion reaction driven by chemical potential difference and the reaction rate is controlled by diffusion. It means sufficient holding time is necessary for Si-18Mn-16Ti-11P master alloy to achieve better refining effect.

Introduction

Electronic packaging is required to provide protection for electronic components from damage, and interconnect between chip and other components while, in the meantime, thermal expansion matching up with electronic components and high thermal conductivity are necessary for avoiding chip failing during circuit operation [1–3]. However, with the integrated circuit (IC) size decreasing and power density continually increasing, it is estimated that 30% computing power of chip is limited by electronic packaging materials [4,5]. One of the limited factors is that mismatch of the coefficient of thermal expansion (CTE) between chip and packaging material. It causes thermal stress fatigue and results in chip failure [6–8]. At the same time, large amounts of heat produced by countless, tiny size electronic components can also make chip overheating to fail because of low thermal conductivity (TC) [9,10]. Thus, it has become very important to develop electronic packaging materials with CTE and TC matching those of the chip. Moreover, lightweight and small size trends require packaging materials have low density and exceptional mechanical properties [11–13].

Metal matrix electronic packaging materials possess matched CTE and high TC to overcome above problems. But conventional metal electronic packaging materials, like Invar alloy (Fe-Ni) and Kovar alloy (Fe-Ni-Co), have too high density to meet lightweight requirements [6]. Therefore, for decades, hypereutectic Al-Si alloys have attracted considerable attention to electronic packaging application because of their excellent integrated performance such as high TC, low CTE, low density and exceptional mechanical properties, etc [14–17]. However, the application of unrefined hypereutectic Al-Si alloy is limited because of irregular, coarse and brittle primary Si which results in poor performance [11,18,19]. Therefore, primary Si must be refined to improve performance of hypereutectic Al-Si alloys for further application.

In recent years, more and more attentions have been paid to refine primary Si and to achieve uniform distribution of microstructures. Among these methods, the spray forming technology has the most extensively investigation [17–20]. But it still has some insufficiency limiting its further application, such as high production cost and low densification for needing subsequent densification processing [19,21]. With the exception of the spray forming technology, friction stir processing, spark plasma sintering, pressure infiltration, powder metallurgy and melting and casting technology have also been studied but still in test stage so far [5,6,13,14,22–24]. Comparing with other methods, melting and casting technology has some advantages, such as simple operation

* Corresponding authors.
E-mail addresses: wuyuying@sdu.edu.cn (Y.-Y. Wu), xfliu@sdu.edu.cn (X.-F. Liu).

http://dx.doi.org/10.1016/j.rinp.2016.10.006
2211-3797/

and low production cost, etc. At present, P refinement is the most popular method in refining primary Si for as-cast hypereutectic Al-Si alloys. Sun et al. [11] have investigated the refinement of Al-50% Si alloy by adjusting superheat temperatures and phosphorus contents, which indicates mechanical properties of hypereutectic Al-Si alloy can be obviously improved by P refinement. Liu et al. [22] have reported that primary Si in hypereutectic Al-24%Si alloy can be refined to 19 μm by addition of P-containing master alloy. However, rare attention has been paid to a generation process of AlP, which can act as heterogeneous nucleus for Si and a key of refining primary Si [25–27]. Moreover, the data on P refinement in high-Si Al-Si alloys (containing more than Al-24%Si) is still scarce and the refining process is still immature, needing further studies.

Although conventional Cu-P, Al-P master alloys have been developed to refine hypereutectic Al-Si alloys, there still exists inconvenience to improve. In industry, Cu-P master alloys have usually been used to refine Cu-containing Al-Si alloys [28]. Because of high density, Cu-P alloys are easy to sink, performing unstable refinement efficiency [28,29]. Al-P master alloys are high-efficiency and environmentally friendly in refinement process of Al-Si alloys. However, due to the low content of P, it needs relatively high addition amount to refine high-Si Al-Si alloys [11,30], which is easy to cause problems during refinement process.

In this work, a new Si-18Mn-16Ti-11P master alloy, with high P content and low density, has been developed. Ti element, containing in the master alloy, can act as alloying element to improve mechanical properties of Al-Si alloy [31]. The microstructure has been characterized and a transformation process of TiP to AlP has been analyzed. The initial and final reaction stages were studied by controlling the reaction time, which helped to build a reaction model to reveal a generation mechanism of AlP. Additionally, the refining effect of Si-18Mn-16Ti-11P master alloy on size, morphology and distribution of primary Si in as-cast Al-27Si alloy was compared to that of Cu-14P and Al-3P alloys for determining the most suitable master alloy on refining hypereutectic Al-Si alloys for electronic packaging applications. Subsequently, influences of P refinement on CTE and mechanical properties of Al-27Si alloys were investigated, which lays a foundation for high-Si Al-Si alloy refined by P for electronic packaging.

Experimental procedure

Al-27Si alloy was prepared using 99.7% commercial purity Al (all compositions quoted in this work are in wt.% unless otherwise stated) and 99.9% crystalline Si. Si-18Mn-16Ti-11P master alloy was prepared using Si-P alloy and titanium sponge in high frequency induction furnace. Si-P, Cu-14P and Al-3P alloys were provided by Shandong Al & Mg Melt Technology Co. Ltd.

For characterizing the transformation process of TiP to AlP, 30% Si-18Mn-16Ti-11P master alloy (i.e. 3.3% P) was added into Al-Si melt, which was prepared in a clay bonded graphite crucible heated by 25 kW medium frequency induction furnace at 850 °C. After the master alloy dissolving in the melt, part of melt was poured into a pre-heated (150 °C) cast iron chill mold immediately and the remained melt was cooled by furnace-cooling.

For comparing the refinement effect of different P-containing master alloys, Al-27Si alloy has been chosen as the experimental subject. The Al-27Si alloy was also prepared in a clay bonded graphite crucible heated by 25 kW medium frequency induction furnace at 880 °C and 350 ppm P was added via Si-18Mn-16Ti-11P, Al-3P and Cu-14P master alloys, respectively. At the meantime, corresponding commercial purity Al and crystalline Si were added in melts for avoiding severe fluctuation of Si content. Subsequently 0.5% C_2Cl_6 was utilized to remove slag and degassing from melt at 850 °C. Before casting, the melt was held at 850 °C for 20 min. Also, another group without P addition was obtained in the same method as above. The prime chemical compositions of the experimental Al-27Si alloys are shown in Table 1.

The Al-27Si alloy refined by Si-18Mn-16Ti-11P master alloy was machined to 'dog-bone' type specimens according to the GB/T228-2002 standard [32] to obtain tensile test bars. The ultimate tensile strengths (UTS) and elongation were carried out using a universal material test machine (CMT4204, China) at ambient temperature. In each case, six specimens were tested and the average result has been reported. The CTE was obtained by a dilatometer (NETZSCH DIL 402C), which scanned from room temperature to 350 °C at a rate of 5 °C/min. In each case, five specimens were tested and the rage result has been reported. The density of Al-27Si alloys was measured using the Archimedes method (See Table 2).

For microstructure observation, the specimens were cut from the center of samples, then mechanically ground and polished. Using optical microscope (MX-2005C, HIROX, Japan) for optical investigation, specimens of Al-Si alloys were etched with modified MuraKami's reagent (a mixture of 60 ml distilled water, 10 g sodium hydroxide and 5 g potassium ferricyanide [33]). The software ImageJ was used to count size of primary Si with at last 8 pictures. The microstructures were characterized using field emission scanning electron microscope (FESEM, model SU-70, Japan) with an energy dispersive spectrometry (EDS) attachment and JSM-6610LV scanning electron microscope (SEM). X-ray diffraction (XRD, Rigaku D/max-rB) was used to qualitatively analyze the phase constitution in alloys.

Results and discussion

Microstructure of Si-18Mn-16Ti-11P master alloy

Fig. 1 shows the microstructure and EDS analyses of Si-18Mn-16Ti-11P alloy, in which plate-strip dark grey phase and irregular white phase randomly distribute on black Si matrix. From the EDS results, plate-strip dark grey phase is identified as P-rich phase containing Ti (point 1) and irregular white phase is (Mn, Si) compound (point 2). From the XRD pattern of the Si-18Mn-16Ti-11P alloy, it is found that the plate-strip, dark grey, P-rich phase is TiP which is the only modality of P in this master alloy. Except TiP, there are only Si phase and $Mn_{15}Si_{26}$ in the Si-18Mn-16Ti-11P alloy as shown in Fig. 2. In addition, the melting range of Si-18Mn-16Ti-11P is about 1400 °C ± 30 °C. Due to the high melting range, this Si-18Mn-16Ti-11P master alloy is more suitable for high-Si Al-Si alloy with high melting temperature. However, although the melting range of this master alloy is up 1000 °C, it is a dissolving and diffusion process after adding this master alloy into Al-Si melts. Therefore the transformation process of this master alloy in Al-Si melt is more important for adjustment of processing parameters and achievement of better refinement effect. The bulk density of Si-18Mn-16Ti-11P is about 2.926 g/cm^3. It is much lower than that of Cu-14P (7 ± 0.4 g/cm^3) and close to that of Al-Si alloys. The similar density with Al-Si alloy is help for avoiding partial accumulation of master alloy and maintaining stable refinement effect.

Transformation process of TiP to AlP in Al-Si melt

To clarify a transformation process of TiP to AlP in Al-Si melt, reaction time of TiP in the melt was controlled and the microstructures of different reaction stages were observed, as presented in Fig. 3. Fig. 3(b) shows a start stage of the transformation of TiP to AlP. Comparing with original plate-like TiP in Si-18Mn-16Ti-11P master alloy (Fig. 3(a)), the common portion of TiP and transition

Table 1
Prime chemical compositions of produced Al-27Si alloys (wt.%).

Samples	Si	Cu	Mn	Ti	P	Al
Unrefined	27.28	0.00076	< 0.00030	0.0022	0.0017	Bal.
Refined by Si-18Mn-16Ti-11P	27.46	0.0102	0.0580	0.0516	0.0247	Bal.
Refined by Al-3P	26.65	0.0248	< 0.00030	0.0023	0.0288	Bal.
Refined by Cu-14P	27.17	0.1680	< 0.00030	0.0024	0.0270	Bal.

Table 2
Theoretical and measured density of Al-27Si alloys.

Alloys	Theoretical density (g/cm^3)	Measured density (g/cm^3)	Relative density (%)
Unrefined Al-27Si alloy	2.60	2.58	99.23
Refined by Si-18Mn-16Ti-11P	2.60	2.56	98.46

area presents radial-like. The radial morphology indicates that the reaction of TiP plates with the melt begins from boundary then gradually spreads to interior. As the reaction proceeding, TiP plates are being increasingly disintegrated and the products constantly send out into the melt. At the end of the reaction, products with various morphologies and sizes gather around the corresponding site of original TiP plates due to that the reaction time is too short and too late for products to send out, as illustrated in Fig. 3(c). In Fig. 3(c), one phase exhibits white blocky and the other black punctiform after enough time. Differently from Fig. 3(c) and (d) shows that the products uniformly distributed in matrix. Comparing Fig. 3(c) and (d), it is known that sufficient time is necessary for the reaction to completely finish and the products to send into the melt. That reminds some actions could be taken for achieving better refining effect on primary Si, such like holding for a period of time after adding Si-18Mn-16Ti-11P master alloy into melt or adding Si-18Mn-16Ti-11P master alloy into Al melt before addition Si during preparing Al-Si alloy. It has a guiding significance to operation in industry.

Fig. 4 shows detailed component analysis of transition area in early stage. As can be seen, the transition zone between TiP and the melt contains Al, Si, Ti and P elements, manifesting that the reaction has generated. The transition area is radial-like, indicating the products will spread into the melt as the reaction. Fig. 5 shows the XRD pattern and EDS analysis of the alloy with the reaction finishing completely. From Fig. 5(a), a new kind of (Al, Ti, Si) compound appears while there is no diffraction peaks of TiP or $Mn_{15}Si_{26}$ but those of Si (AlP) and $Al_{57}Mn_{12}$, It reveals that the transformation of TiP to AlP has completely finished. Except a diffraction peak corresponding with (420) of AlP, the diffraction peaks of AlP phase overlap those of Si due to their similar lattice structure [34]. The diffraction peak corresponding with (420) of AlP was magnified in the upper right corner of Fig. 5(a). To more clearly characterize the reaction products, Fig. 3(d) was been magnified and EDS analysis has been conducted as shown in Fig. 5(b). The result figures the black particles are AlP (point 1) and the light grey blocks are ternary (Al, Ti, Si) compounds (point 2). The element O was also detected due to the oxidation of AlP during the sample preparation process [35]. In addition, the AlP particles are larger because excess Si-18Mn-16Ti-11P master alloy (amount to 3.3% P addition) has been added into the melt for clearly observing a process of the transformation of TiP to AlP, compared to a typical addition of 350 ppm P.

Mechanism of the transformation of TiP to AlP

According to above observations, it can be inferred that when Si-18Mn-16Ti-11P master alloy is added into the melt, Si matrix of the master alloy dissolves firstly, leading to TiP exposure in the melt and directly contacting with Al atoms. Then a liquid-solid diffusion reaction occurs. The direct evidence is provided by element distribution along A-B in Fig. 6(a) and (b). According to the distribution of Al element as shown in Fig. 6(b), the concentration of Al element in the melt is much higher than that in TiP. The concentration gradient drives Al atoms to diffuse into TiP and then generating a gradually decreasing concentration gradient from boundary to center. Similarly, gradually decreasing concentration gradient of Ti and P elements from center to boundary is observed, illustrating that the products tend to spread out as the diffusion reaction. Moreover, the distribution of Si element mainly uniforms in transition area, indicating that dissociating Si atoms did not totally diffused into the melt and part of them gather around the boundary of TiP particle.

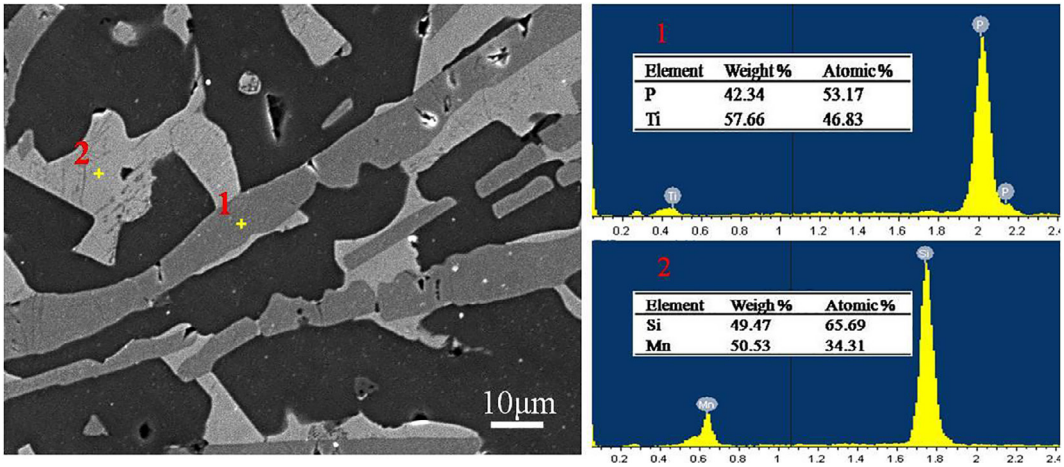

Fig. 1. Microstructure and EDS analysis of Si-18Mn-16Ti-11P master alloy.

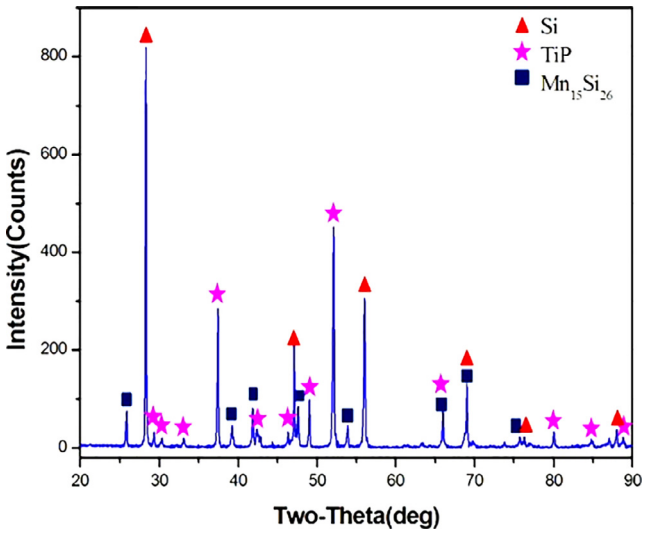

Fig. 2. XRD pattern of Si-18Mn-16Ti-11P master alloy.

To simply describe the liquid-solid diffusion reaction of TiP with the melt, the transition area is divided into four parts as marked in Fig. 6(c) according to difference of elements distribution. A core-shell reaction model has been established, as displayed in Fig. 7, to present the reaction schematic. As is known to all, different chemical potential between various compounds is the driving force of a physical process [36]. Atoms will diffuse from higher chemical potential phase to lower due to the interaction between homogeneous and heterogeneous atom groups and the principle of entropy increase. When TiP is bare in the melt, the chemical potential of Al in the melt is far higher than that in TiP compounds, resulting in Al atoms diffusing to TiP compounds according to the positive concentration gradient and then generating a diffusion layer (Fig. 7(a)). Following that, Al atoms swap out Ti atoms on TiP surface and combine with P atoms to form AlP (TiP + Al(l) → AlP + [Ti]). Then Ti atoms combine with other atoms to form intermediate compounds while AlP and Ti atoms spread out. This process is named as inner shell reaction as shown in Fig. 7(b). Subsequently, AlP and intermediate compounds containing Ti keep on spreading, arriving at a rich-Al zone. The intermediate compounds dope with Al atoms to form (Al, Ti, Si) compounds. This process is named as outer shell reaction as presented in Fig. 7(c). Corresponding experimental result is shown in Fig. 6(c). Finally, AlP and (Al, Ti, Si) compounds aggregate and grow up after debonding from reaction interface and distribute in matrix evenly.

In term of dynamics, diffusion controls the reaction rate of TiP with the melt in this experimental condition. Therefore, the kinetic equation of the reaction of TiP with the melt can be expressed by boundary diffusion rate equation [37]:

$$v = DA(c_0 - c)/\delta \quad (1)$$

where v represents the reaction rate, c_0 and c represent the concentration of Al in the melt and reaction layer, respectively, D, A and δ is the diffusion coefficient of Al elements, the surface area of TiP particles and the effective boundary layer thickness, respectively. Base on Eq. (1), some methods of improving the reaction rate can be proposed, such as raising the melting temperature for increasing D (D = f(T)). In industry, a method of enhanced liquid convection by mechanical agitation is feasible. It can not only enlarge the reaction interface, but also reduce the boundary layer thickness via washing action from fluid.

Refining effect in Al-27Si alloys

In following experiment, three kinds of P-containing master alloys have been chosen to compare refining effect on primary Si in Al-27Si alloy. Fig. 8(a) shows that primary Si has varied

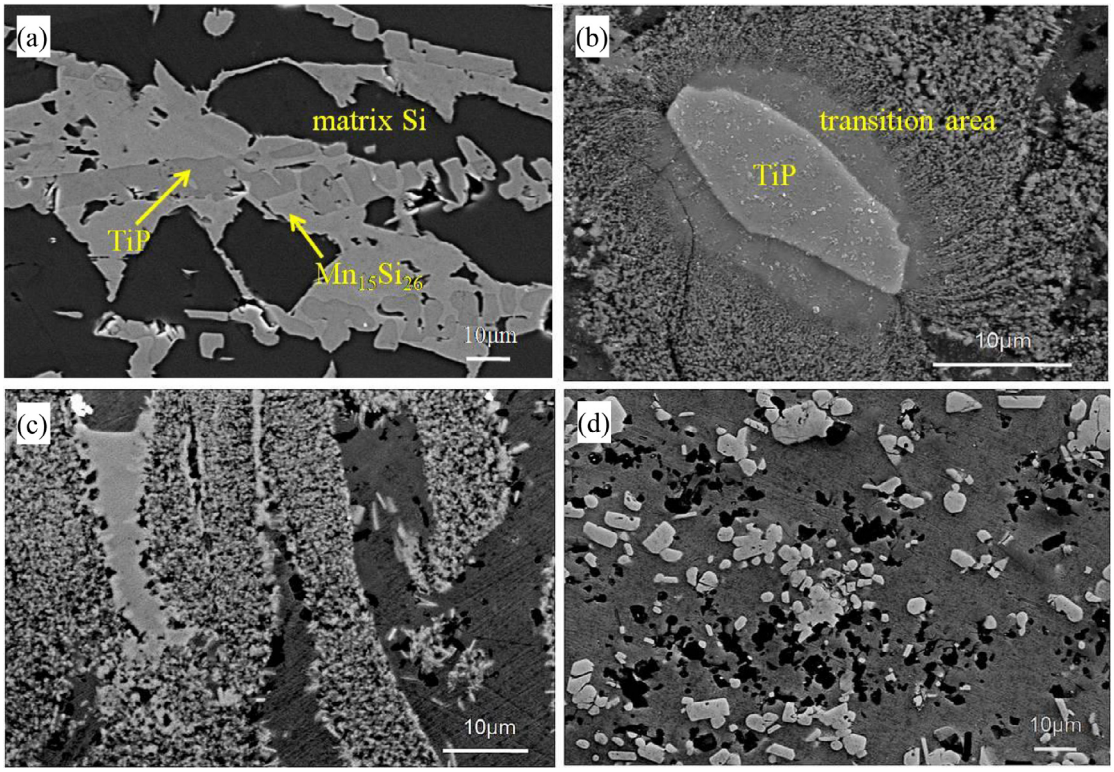

Fig. 3. Evolution of Si-18Mn-16Ti-11P in Al-Si melt: (a) Si-18Mn-16Ti-11P master alloy; (b) start of the reaction; (c) the reaction coming to the end; (d) the reaction finishing.

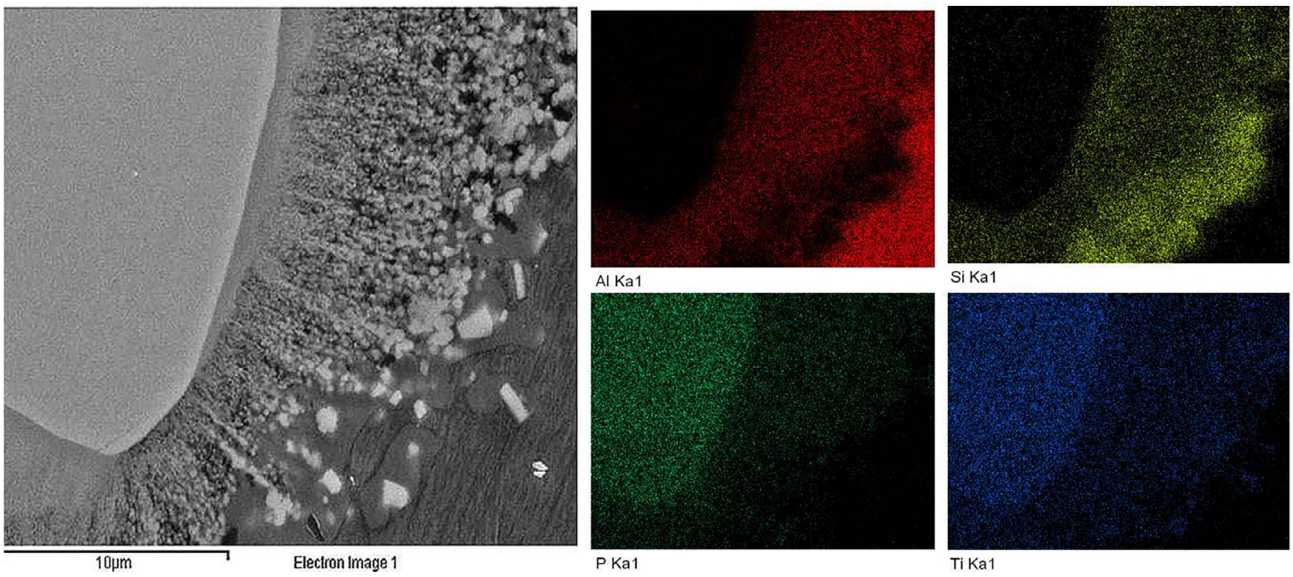

Fig. 4. SEM component analysis at the start stage of the reaction of TiP in Al-Si melt.

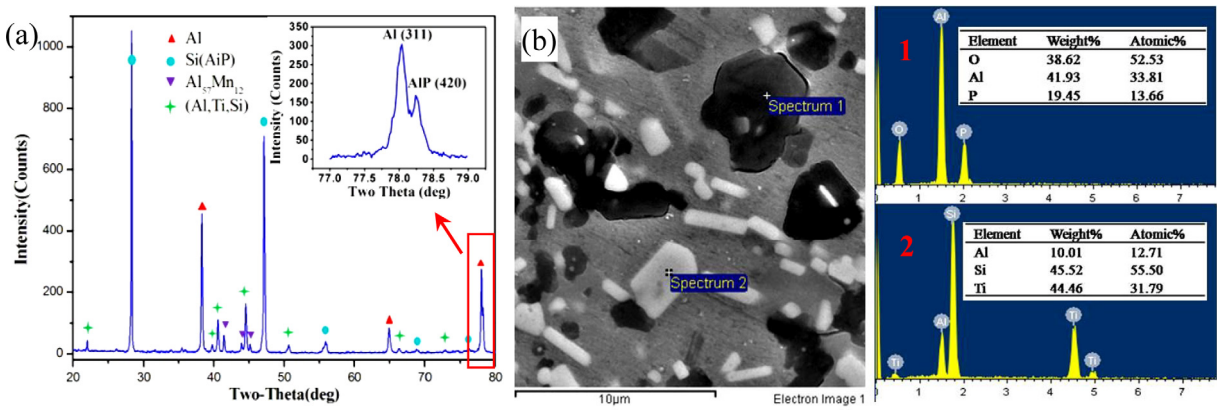

Fig. 5. XRD and EDS analysis of the alloy at end of reaction: (a) XRD pattern; (b) EDS analysis.

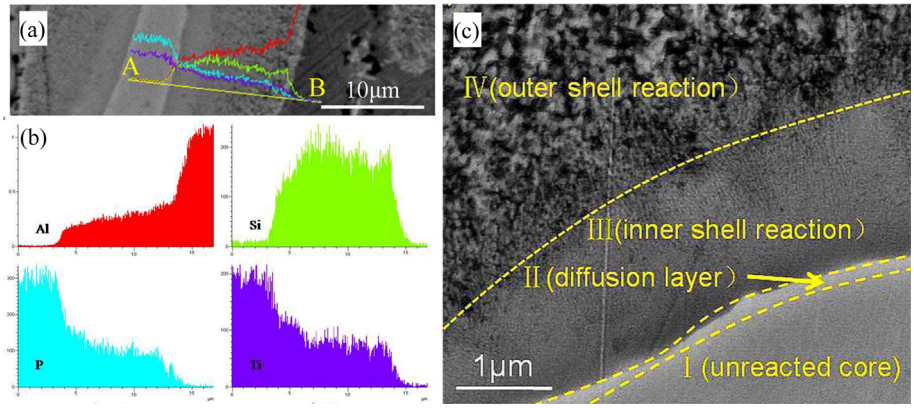

Fig. 6. Microanalysis of element distribution along A-B and microstructure of transition area: (a), (b) EDS scanning results; (c) microstructure.

morphology and size in unrefined Al-27Si alloy, while (b), (c) and (d) present the microstructures of refined alloys by Cu-14P, Al-3P and Si-18Mn-16Ti-11P master alloy, respectively. The original size of primary Si in unrefined Al-27Si alloy is above 488 μm and the average size of refined primary Si reduces to 28.2 ± 1.4 μm, 19.1 ± 2.5 μm and 14.7 ± 1.3 μm via addition of Cu-14P, Al-3P and Si-18Mn-16Ti-11P master alloy, respectively. Except that, the morphology of primary Si becomes into regular block for the sample with Si-18Mn-16Ti-11P and Al-3P addition as well as substantial primary Si presents flower-like for the sample with Cu-14P

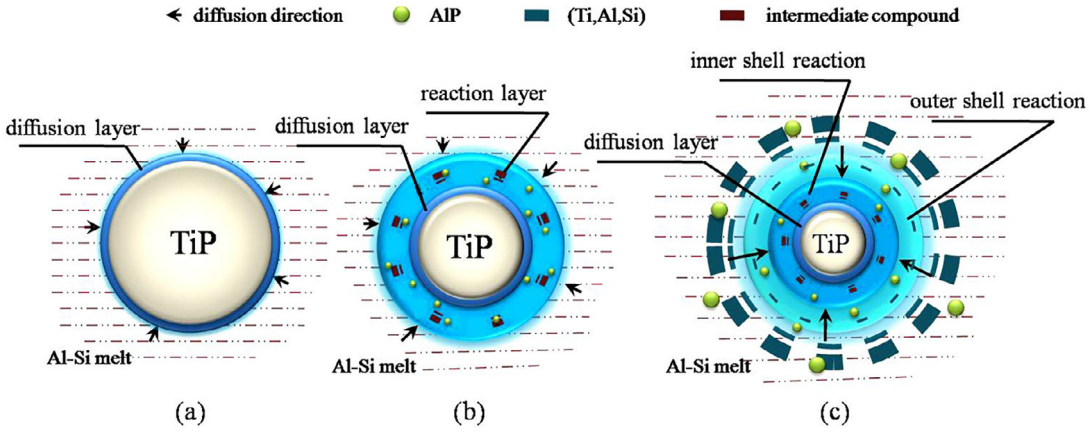

Fig. 7. Schematic illustration of the reaction of TiP with Al-Si melt.

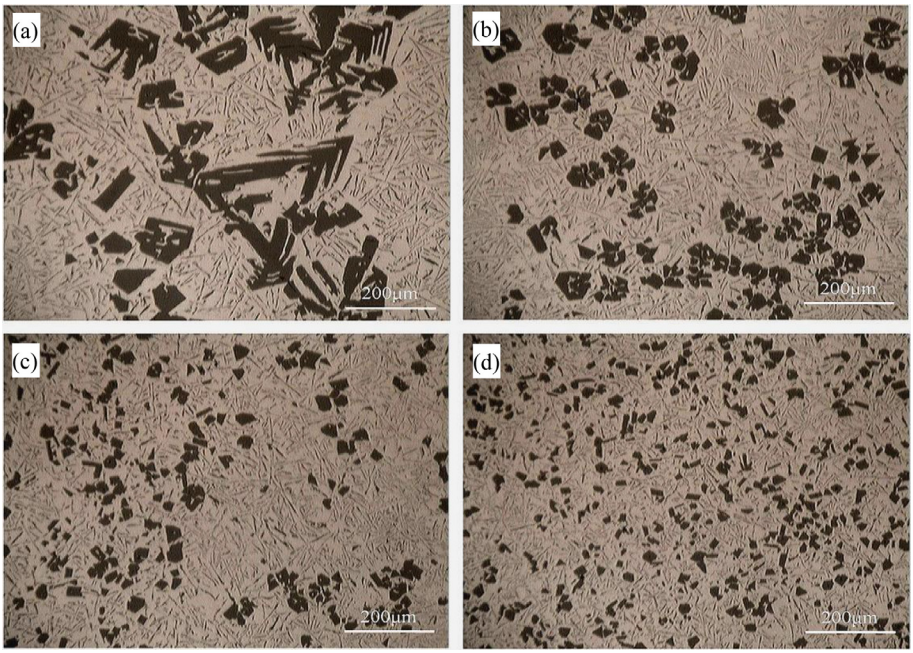

Fig. 8. Microstructures of Al-27Si alloys: (a) unrefined; (b)-(d) refined by Cu-14P, Al-3P and Si-16Ti-11P master alloy, respectively.

addition. Furthermore, the distribution of refined primary Si by Si-18Mn-16Ti-11P master alloy is more uniform than that by Al-3P and Cu-14P. Therefore, considering of size, morphology and distribution of primary Si, the new Si-18Mn-16Ti-11P master alloy is more suitable for Al-27Si alloy than Cu-14P and Al-3P master alloys. It is well-accepted that AlP can act as heterogeneous nucleus of Si and is a key of refining effect on primary Si for P refinement [25–27]. P exists as TiP, AlP, Cu_3P in Si-18Mn-16Ti-11P, Al-3P and Cu-14P alloy, respectively. After adding master alloy into Al-Si melt, phosphorous compounds will transform to AlP. The AlP separating from melt has higher activity of refinement than those of previous addition [34]. Thus, the AlP transforming from TiP has higher activity and the refining effect of Si-18Mn-16Ti-11P master alloy is better than that of Al-3P master alloy. Moreover, although Cu_3P in Cu-14P master alloy also transforms to AlP which has high activity too, Cu-14P master alloy would sink in Al-Si melt and separating AlP is apt to segregation because of the density of Cu-14P master alloy much higher than Al-Si melt. As a result, the refining effect of Cu-14P is worse than that of Si-18Mn-16Ti-11P.

Influence of P refinement on CTE and tensile properties in Al-27Si alloys

The influence of P refinement on the coefficient of thermal expansion (CTE) and the tensile properties of Al-27Si alloy were investigated in this work. An average CTE in the temperature range of 40–150 °C has been reduced from 18.6616.25 $\times 10^{-6}$/K to 16.25 $\times 10^{-6}$/K before and after P refinement, indicating that the influence of P refinement on CTE is positive. In addition, the CTE value of refined Al-27Si alloy is just slightly higher than that of CE17 (Al-27Si alloy) produced by Osprey Metals Ltd. using the Osprey spray deposition process [21]. It demonstrates P refinement may be a candidate for refining hypereutectic Al-Si alloy for electronic packaging applications. Fig. 9 presents the CTE values with varying temperature for the Al-27Si alloys before and after P refinement at 150–350 °C. It can be also observed that, within the entire temperature range, P refinement process significantly reduces the CTE.

In terms of the rule of mixture (ROM), the CTE is affected by complex factors, such as alloy composition, solubility of elements,

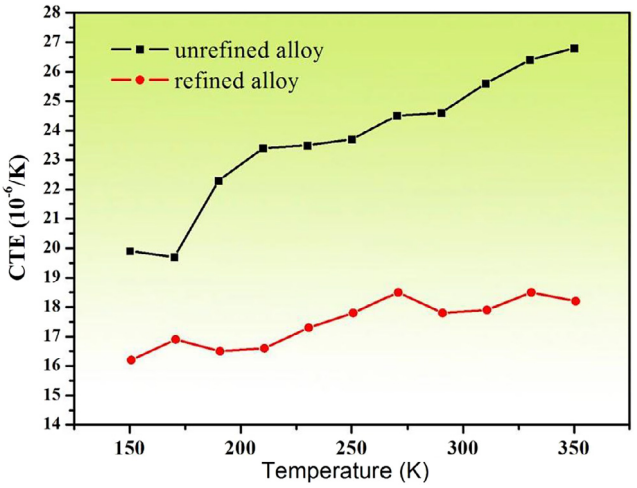

Fig. 9. CTE curves of Al-27Si alloys before and after P refinement by Si-18Mn-16Ti-11P alloy.

density, precipitated phase and operating process, etc. In this work, only distribution and morphology of primary Si as well as the density of Al-27Si alloy were discussed. The CTE value of Al and Si is 2.26×10^{-5}/K and 2.5×10^{-6}/K, respectively. The difference of the CTE value between Al and Si is an order of magnitude [23]. Hence, the CTE value of Al-Si alloy with a high content Si is mainly affected by Si. With an increasing temperature, ductile Al matrix and brittle Si particles will both expand. But Al matrix is easier to come about plastic deformation due to the CTE value of Al matrix is much higher than that of Si. In unrefined Al-27Si alloy, brittle primary Si is coarse and uneven distribution, resulting in ductile Al matrix mutual continuation as shown in Fig. 8(a). When ductile Al matrix is in continuous condition, its deformation will be less restrained by the surrounding brittle Si particles. After P refinement, small and regular primary Si besets in Al matrix evenly, as presented in Fig. 8(d). It has a relatively bigger restraint on expansion of Al matrix. As a result, the refined Al-27Si alloy has a lower CTE. Moreover, the density of Al and Si is 2.7 and 2.33 g/cm^3, respectively [23]. The theoretical density obtained through the ROM and the measured densities of Al-27Si alloys are illustrated in Table 1. After refinement, the density of Al-27Si alloy decreases. This abnormal phenomenon may be attributed to gas involved in melt during the process of refining. According to the investigations reporting that refinement of the reinforcement particles and large amount of porosity could decrease the CTE [6,38]. The decreased density of the refined alloy may be another reason for the reduction of the CTE.

The tensile properties of Al-27Si alloys before and after P refinement are shown in Fig. 10. From the results in Fig. 10, both the UTS and elongation of the refined Al-27Si alloy are obviously improved. The UTS and elongation of Al-27Si alloys before and after refinement are about 71.5 MPa, 147 MPa and 0.31%, 1.04%, respectively, agreeing well with the refining performance. Comparing with the unrefined Al-27Si alloy, the UTS of the refined alloy is increased by 106% and elongation is increased by 235%. Although the tensile properties of Al-27Si alloy are improved, it is still lower than that of alloys prepared by rapid solidification [23,24]. It may be attributed to low compactness of alloys prepared in this experimental condition (Table 1). Moreover, in this work, the Al-27Si alloys are as-cast state without heat treatment. After heat treatment, the alloys are expected to perform better in tensile properties [11,20]. In addition, tensile strength depends on matrix and reinforcement [39]. For hypereutectic Al-Si alloy, the strength is closely related to size, morphology and distribution of primary Si [40]. Smaller size of primary Si, more regular morphology and more homogeneous distribution are more beneficial to tensile properties.

The fracture surfaces of Al-27Si alloys are shown in Fig. 11. The fracture of Al-27Si alloy is brittle as a whole, according to that the fracture plane is vertical to a tensile direction with no visible macro-ductility, as presented in Fig. 11(a) and (c). Moreover, clear cleavage plane can also be seen from Fig. 11(a) and (c) due to the brittle nature of Si particle. However, no visible interfacial debonding is observed, revealing an excellent interfacial bonding strength between Si particles and Al matrix. It is usual to find interfacial debonding between Si particles and Al matrix in hypereutectic Al-Si alloy fabricated by infiltration or filtration squeeze casting without subsequent processing [6,15]. Differently, Si particles separating from melt have better interfacial bonding with Al matrix. That is beneficial to mechanical properties. In addition, a large number of cracks are found on coarse primary Si particles in Fig. 11(a) and crushing Si particle is illustrated in Fig. 11(b). According to Smith Theory [36], due to elastic modulus of Si particle higher than Al matrix, Al matrix tends to come about plastic deformation and the stress tends to gather to the interface between Si particles and Al matrix when a force applied on Al-27Si alloy. With the increase of tension, the increasing stress results in the generation of cracks and crush of Si particles. In addition, the unrefined primary Si particles have sharp edge angles, which is usually the place of the stress concentration. The sharp edge angles tend to split Al matrix with increasing stress and results in alloy fracture. In Fig. 11(c) and (d), there are no crushing Si particles but some small cracks on the fracture surface of the refined Al-27Si alloy. It indicates that the stress concentration has been lessen, which avoiding Si crushing. Furthermore, dimples left on the fracture surface of the refined Al-27Si alloy demonstrate that Al matrix undergoes a bit of plastic deformation before fracture. The dimples, which are not found in unrefined Al-27Si alloy, reveal that refined Al-27Si alloy has better malleability, which coinciding with the tensile test results (Fig. 9). That is to say, small, regular and even distributing primary Si is a key of high tensile properties. That is a reason that better refining effect of primary Si is required.

Conclusions

A novel Si-18Mn-16Ti-11P master alloy has been developed to refine Al-27Si for lower CTE and better tensile properties. Moreover, the microstructure of Si-18Mn-16Ti-11P alloy and the generation process of AlP in Al-Si melt were characterized in detail with a core-shell reaction model. The following conclusions can be drawn:

(1) After addition of 350 ppm P via Si-18Mn-16Ti-11P master alloy, primary Si in Al-27Si alloy was refined from coarse plate (above 488 μm) to regular block (14.7 ± 1.3 μm). Comparing with Cu-14P and Al-3P, Si-18Mn-16Ti-11P performed more excellent refining effect on primary Si with smaller size, more regular morphology and more uniform distribution. It indicates the new Si-18Mn-16Ti-11P master alloy is more suitable for high-Si alloys (more than 24% Si) than Cu-14P and Al-3P master alloys.

(2) P refinement is beneficial to reduction of CTE and enhancement of tensile properties of Al-27Si alloy. For refined Al-27Si alloy by Si-18Mn-16Ti-11P, a CTE of 16.25×10^{-6}/K, an increased UTS and elongation by 106%, 235% than those of unrefined alloy were obtained respectively. The CTE value is just slightly higher than that of Si_p/Al composites fabricated by spray deposition, indicating P refinement

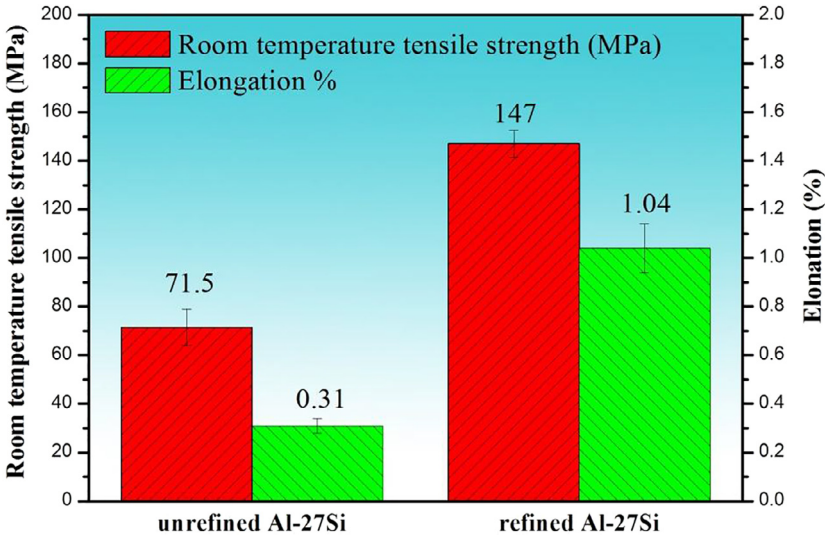

Fig. 10. UTS and elongation of Al-27Si alloys before and after P refinement by Si-18Mn-16Ti-11P master alloy.

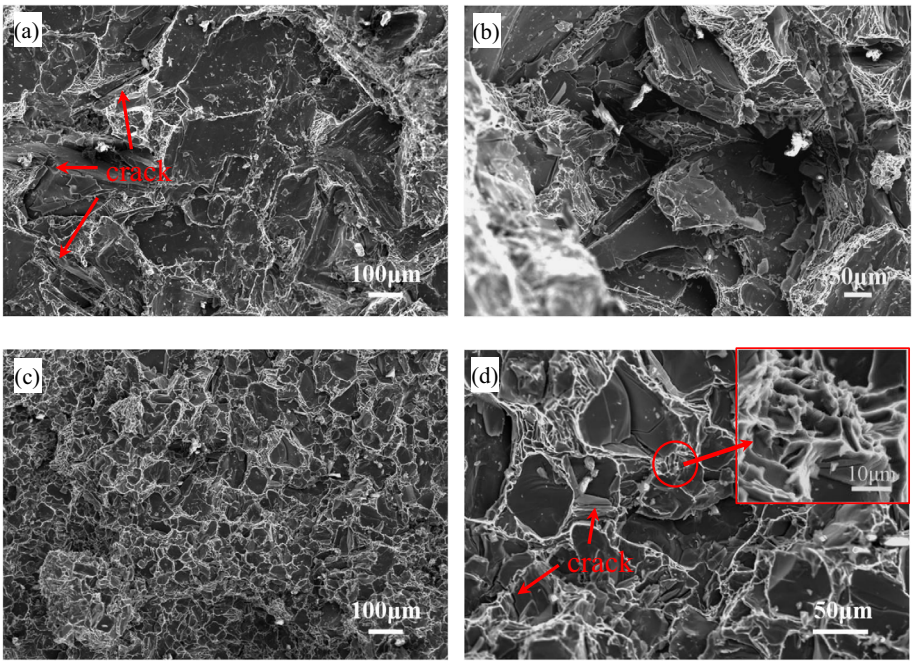

Fig. 11. Fracture morphologies of Al-27Si alloys: (a), (b) unrefined; (c), (d) refined by Si-18Mn-16Ti-11P master alloy.

may be a candidate for refining hypereutectic Al-Si alloy for electronic packaging applications.

(3) The only one form of P is plate-strip TiP in Si-18Mn-16Ti-11P alloy. A core-shell reaction model was established to reveal the mechanism of the liquid-solid diffusion reaction of TiP with Al-Si melt, driven by chemical potential difference. Due to the reaction rate is controlled by diffusion and it needs time for products to spread evenly, sufficient holding time is necessary for Si-18Mn-16Ti-11P master alloy to achieve better refining effect.

Acknowledgements

This work is supported by the National Natural Science Foundation of China (Nos. 51571133, 51001065) and the Young Scholars Program of Shandong University (YSPSDU).

References

[1] Chu K, Jia CC, Liang XB, Chen H, Guo H. The thermal conductivity of pressure infiltrated SiC_p/Al composites with various size distributions: experimental study and modeling. Mater Des 2009;30:3497–503.
[2] Zhang QG, Gu MY. Effect of silicon carbide particles on properties of Al/Si_p + SiC_p. Mater Sci Eng A 2006;419:86–90.
[3] Yu K, Li SJ, Chen LS, Zhao WS, Li PF. Microstructure characterization and thermal properties of hypereutectic Si-Al alloy for electronic packaging applications. Trans Nonferrous Met Soc China 2012;22:1412–7.
[4] Germen RM, Hens KF, Johnson JL. Powder metallurgy processing of thermal management materials for microelectronic applications. Int J Powder Metall 1994;30:205–15.
[5] Jacobson DM. Lightweight electronic packaging technology based on spray formed Si-Al. Powder Metall 2000;43:200–2.
[6] Chien CW, Lee SL, Lin JC, Jahn MT. Effects of Si size and volume fraction on properties of Al/Si_p composites. Mater Lett 2002;52:334–41.
[7] Ni ZL, Zhao HJ, Mi PB, Ye FX. Effect of sintering time on the bending strength and CTE of SiC/Al-35Si composite. Vacuum 2016;124:28–31.
[8] Zhang QG, Zhang HX, Gu MY, Jin YP. Studies on the fracture and flexural strength of Al/Si_p composite. Mater Lett 2004;58:3545–50.

[9] Cho JW, Goodson KE. Cool electronic. Nat Mater 2015;14:136–7.
[10] Wei ZJ, Ma P, Wang HW, Zou CM, Scudino S, Song KK, Prashanth KG, Jiang W, Eckert J. The thermal expansion behaviour of SiC_p/Al-20Si composites solidified under high pressures. Mater Des 2015;65:387–94.
[11] Cao FY, Jia YD, Prashanth KG, Ma P, Liu JS, Scudino S, Huang F, Eckert J, Sun JF. Evolution of microstructure and mechanical properties of as-cast Al-50Si alloy due to heat treatment and P modifier content. Mater Des 2015;74:150–6.
[12] Shaga A, Shen P, Sun C, Jiang QC. Lamellar-interpenetrated Al–Si–Mg/SiC composites fabricated by freeze casting and pressureless infiltration. Mater Sci Eng A 2015;630:78–84.
[13] Yu JH, Wang CB, Shen Q, Zhang LM. Preparation and properties of Si_p/Al composites by spark plasma sintering. Mater Des Mater Des 2012;41:198–202.
[14] Rao AG, Deshmukh VP, Prabhu N, Kashyap BP. Ductilizing of a brittle as-cast hypereutectic Al–Si alloy by friction stir processing. Mater Lett 2015;159:417–9.
[15] Zhang WL, Ding DY, Gao P. High volume fraction Si particle-reinforced aluminium matrix composites fabricated by a filtration squeeze casting route. Mater Des 2016;90:834–8.
[16] Kang N, Coddet P, Liao HL. Macrosegregation mechanism of primary silicon phase in selective laser melting hypereutectic Al-high Si alloy. J Alloys Compd 2016;662:259–62.
[17] Hogg SC, Lambourne A, Ogilvy A, Grant PS. Microstructural characterisation of spray formed Si-30Al for thermal management applications. Scripta Mater 2006;55:111–4.
[18] Zhang L, Gan GS, Yang B. Microstructure and property measurements on in situ TiB_2/70Si-Al composite for electronic packaging applications. Mater Des 2012;36:177–81.
[19] Jia YD, Cao FY, Scudino S, Maa P, Li HC, Yu L, Eckert J, Sun JF. Microstructure and thermal expansion behavior of spray-deposited Al-50Si. Mater Des 2014;57:585–91.
[20] Zhu XW, Wang RC, Peng CQ, Liu WS, Peng J. Microstructure and thermal expansion behavior of spray-formed Al-27Si alloy used for electronic packaging. J Mater Sci Mater Electron 2014;25:4889–95.
[21] Jacobson DM, Ogilvy AJW. Spray-deposited Al–Si (Osprey CE) alloys and their properties. Mat wiss u Werkstofftech 2003;34:381–4.
[22] Wu YP, Wang SJ, Li H, Liu XF. A new technique to modify hypereutectic Al-24% Si alloys by a Si-P master alloy. J Alloys Comp 2009;477:139–44.
[23] Cai ZY, Zhang C, Wang RC, Peng CQ, Qiu K, Feng Y. Preparation of Al–Si alloys by a rapid solidification and powder metallurgy route. Mater Des 2015;87:996–1002.
[24] Cai ZY, Wang RC, Zhang C, Peng CQ, Wang LQ. Microstructure and properties of Al/Si_p composites for thermal management applications. J Mater Sci Mater Electron 2015;26:4234–40.
[25] Ho CR, Cantor B. Heterogeneous nucleation of solidification of Si in Al–Si and Al–Si–P alloys. Acta Metall Mater 1995;43:3231–46.
[26] Eiken J, Apel M, Liang SM, Schmid-Fetzer R. Impact of P and Sr on solidification sequence and morphology of hypoeutectic Al–Si alloys: Combined thermodynamic computation and phase-field simulation. Acta Mater 2015;98:152–63.
[27] Liang SM, Schmid-Fetzer R. Phosphorus in Al–Si cast alloys: thermodynamic prediction of the AlP and eutectic (Si) solidification sequence validated by microstructure and nucleation undercooling data. Acta Mater 2014;72:41–56.
[28] Robles Hernández FC, Sokolowski JH. Comparison among chemical and electromagnetic stirring and vibration melt treatments for Al–Si hypereutectic alloys. J Alloys Comp 2006;426:205–12.
[29] Zhang HH, Duan HL, Shao GJ, Xu LP. Microstructure and mechanical properties of hypereutectic Al–Si alloy modified with Cu–P. Rare Met 2008;27:61–3.
[30] Zhang Q, Liu XF, Dai HS. Re-formation of AlP compound in Al-Si melt. J Alloys Comp 2009;480:376–81.
[31] Gao T, Zhang YR, Liu XF. Influence of trace Ti on the microstructure, age hardening behavior and mechanical properties of an Al–Zn–Mg–Cu–Zr alloy. Metall Mater Trans A 2014;598:293–8.
[32] GB/T228-2002. Metallic materials-tensile testing at ambient temperature. China Standard Press; 2002.
[33] Timpel M, Wanderka N, Grothausmann R, Banhart J. Distribution of Fe-rich phases in eutectic grains of Sr-modified Al-10wt.%Si-0.1wt.%Fe casting alloy. J Alloys Comp 2013;558:18–25.
[34] Bao GJ, Li DK, Nie JF, Liu XF. The phase transition of ZrP induced by Si in Al–Si melts. J Alloys Comp 2012;528:45–50.
[35] Cho YH, Lee HC, Oh KH, Dahle AK. Effect of strontium and phosphorus on eutectic al-si nucleation and formation of β-al_5fesi in hypoeutectic Al–Si foundry alloys. Metall Mater Trans A 2008;39:2435–48.
[36] Hu GX, Cai X, Rong YH. Fundamentals of materials science. 4th ed. Shanghai: Shanghai Jiao Tong University Press; 2011.
[37] Cheng LZ. Physical chemistry. 4th ed. Shanghai: Shanghai Scientific & Technical Publishers; 2007.
[38] Elomari S, Skibo MD, Sundarrajan A, Richards H. Thermal expansion behavior of particulate metal-matrix composites. Compos Sci Technol 1998;58:369–76.
[39] Beffort O, Long SY, Cayron C, Kuebler J, Buffat PA. Alloying effects on microstructure and mechanical properties of high volume fraction SiC-particle reinforced Al-MMCs made by squeeze casting infiltration. Compos Sci Technol 2007;67:737–45.
[40] Maeng DY, Lee JH, Won CW, Cho SS, Chun BS. The effects of processing parameters on the microstructure and mechanical properties of modified B390 alloy in direct squeeze casting. J Mater Process Technol 2000;105:196–203.